

## TRANSMISSION ELECTRON MICROSCOPY STUDY OF Ge NANOPARTICLES FORMED IN GeSiO FILMS BY ANNEALING IN HYDROGEN

V. S. TEODORESCU, A. V. MARALOIU, I. STAVARACHE,  
A.-M. LEPADATU, M. L. CIUREA \*

*National Institute of Materials Physics, 105 bis Atomistilor Street, Magurele  
077125, Romania*

This paper presents a detailed transmission electron microscopy (TEM) study of GeSiO films with Ge nanoparticles. The films with 2.5  $\mu\text{m}$  thickness were deposited by magnetron sputtering and subsequently annealed in  $\text{H}_2$  at 2 atm and 500  $^\circ\text{C}$  for 2 h for nanostructuring. After  $\text{H}_2$  annealing, the majority of the resulted Ge nanoparticles are amorphous, less than 5 nm in size, forming a uniform network in the film volume. Big Ge nanoparticles with sizes between 20 and 50 nm are also formed. Some of them are identified to be crystallized in the (Ge-III/ST12) tetragonal phase. The high resolution TEM observation induces the amorphysation of the Ge tetragonal phase, followed by the crystallization of the amorphous Ge phase in the cubic diamond structure (Ge-I), as an effect of electron irradiation. A secondary annealing performed in  $\text{N}_2$  at 800  $^\circ\text{C}$  and 1 atm for 2 h induces formation of faceted cubic Ge nanoparticles distributed in the  $\text{SiO}_2$  matrix.

(Received November 4, 2013; Accepted November 27, 2013)

*Keywords:* Ge nanoparticles; Ge-III/ST12 phase; Magnetron sputtering; TEM; HRTEM; Electron irradiation.

### 1. Introduction

The thin films of Ge nanoparticles embedded in amorphous  $\text{SiO}_2$  matrix are extensively studied for their photoelectric [1–3] and photoluminescent [4–6] properties and also for memory effect [6–8]. This system can be obtained by several methods: co-sputtering from Ge and  $\text{SiO}_2$  targets (or Ge pieces attached to  $\text{SiO}_2$  target) [9–15], Ge ions implantation in  $\text{SiO}_2$  layers [16–19], sputtering the  $\text{SiO}_2/\text{Ge}/\text{SiO}_2$  multilayered structures [20–24], sol gel [13, 25–28].

All the films prepared by any of these methods are annealed for the formation of Ge nanoparticles. The resulted structure and morphology of the GeSiO films depend on the manufacturing method and annealing history. The evolution of films structure due to the annealing can be observed in detail at nanometric scale by transmission electron microscopy (TEM), specially using the cross-section TEM (XTEM) specimen preparation method.

In the most papers reported on Ge nanocrystals embedded in  $\text{SiO}_2$  matrix, the XTEM observations reveal only amorphous and cubic diamond structures of Ge [20, 29]. Ge-III/ST12 phase was found in high pressure studies in both Ge bulk and thin films [30–32]. However, the Ge-III structure was found at ambient pressure in free Ge nanoparticles (powders) prepared by the naphthalide-mediated reduction of  $\text{GeCl}_4$  treated with t-BuMgCl [33]. Ge nanoparticles with tetragonal structure (Ge-III/ST12) were also evidenced in thick GeSiO films annealed in  $\text{H}_2$  atmosphere (2 atm and 500  $^\circ\text{C}$ ) [13] by using TEM measurements. For this, microfragments were mechanically extracted from the film surface using a thin diamond tip [34] which can be suspected to trigger the formation of high pressure phases, similarly to the diamond indentation measurements [35, 36].

---

\* Corresponding author: ciurea@infim.ro

One of the problems concerning the GeSiO system is the generation mechanism of the stress field during the annealing process performed for Ge nanocrystals formation. In GeSiO films obtained by Ge ions implantation in SiO<sub>2</sub> films, the initial stress field produced during the implantation process is relaxed by annealing [37]. In other case, also in implanted films, some compressive stress is found from Raman studies [38]. In these two cases, no Ge-III high pressure phase was reported. The compressive stress, strongly dependent on the annealing temperature and Ge concentration is also reported [39] in films with Ge nanocrystals embedded in SiO<sub>2</sub> prepared by co-sputtering followed by annealing. In this case, the compressive stress has the value of about 1 GPa, which is much less than the values corresponding to the formation of the Ge-III high pressure phase in bulk Ge [31, 32].

In the present study, we aim to explain the presence of the Ge-III phase in the samples annealed in H<sub>2</sub> and to elucidate if this phase is induced or not by preparation of TEM specimen using the microfragment extraction preparation method. For this, all the TEM specimens are prepared by the conventional cross-section method and a detailed XTEM study is performed.

## 2. Experimental details

The GeSiO films were deposited by radio frequency magnetron co-sputtering of SiO<sub>2</sub> and Ge on quartz substrate (more details in Ref. [13]), so that an atomic Ge concentration of about 40 % in the film was obtained. Ge nanoparticles are formed by Ge segregation in SiO<sub>2</sub> matrix during the thermal annealing performed in H<sub>2</sub> at 2 atm and 500 °C for 2 h. The annealed films have about 2.5 μm thickness. A secondary annealing was performed in N<sub>2</sub> at 1 atm and 800 °C for 2 h.

The XTEM method was used for the preparation of TEM specimens. The samples were cut in 0.5 × 2 mm pieces with a diamond wire saw. The pieces were glued face to face with M-bond, and then a mechanical polishing and finally an ion milling in a Gatan PIPS 691 instrument were performed. The conventional TEM measurements were carried out on a JEOL 200CX electron microscope and high resolution TEM (HRTEM) and Energy Dispersive X-ray Spectroscopy (EDX) investigations were made in a JEM ARM200F instrument.

## 3. Results and discussions

The low magnification XTEM image of all film thickness is shown in Fig. 1, which reveals the presence of quite big nanoparticles with round or irregular shape distributed in all the film volume. The EDX measurements made in probe mode on these big nanoparticles show the major presence of Ge. The density of big Ge nanoparticles is not uniform, being higher near the interface with the substrate.

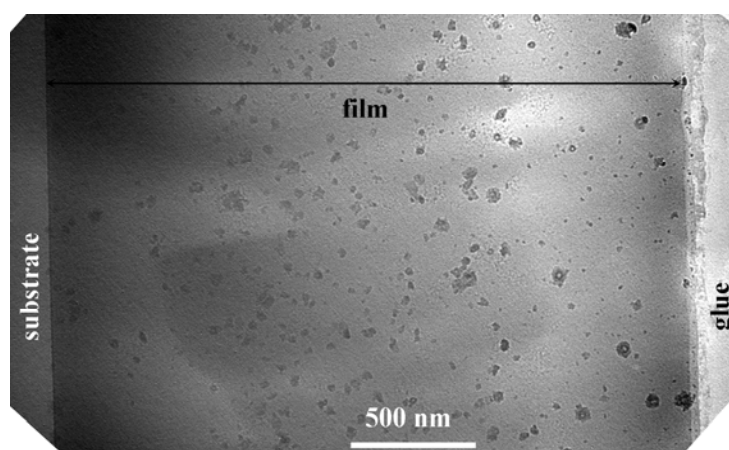
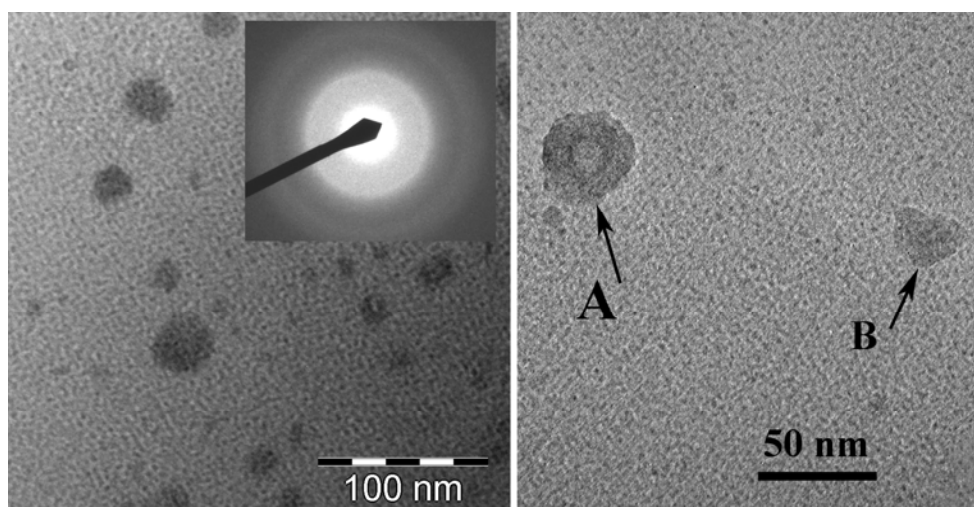


Fig. 1. Low magnification XTEM image of the film.

At intermediate magnification (images in Fig. 2), the big Ge nanoparticles appear in dark contrast with different morphologies, their sizes being between 20 to 50 nm. The round ones show more contrast and are similar with the particles showing tetragonal phase previously observed [13]. Many of these big Ge nanoparticles are amorphous but some of them show traces of crystallinity. However, the SAED patterns recorded on the XTEM specimens indicate an amorphous structure (inset in Fig. 2). A similar morphology of the big Ge nanoparticles was observed in the TEM study performed on microfragments extracted from the film, but in that case the SAED patterns showed spots corresponding to the strong reflexions of tetragonal Ge-III phase. The main spots evidenced in those SAED patterns belong to the (201) reflection (0.27 nm) interplanar spacing, this being the strongest reflection of the tetragonal Ge-III phase [13].



*Fig. 2. Conventional TEM image showing spherical big Ge nanoparticles in a thick area of the XTEM specimen (left). The inset SAED pattern shows an amorphous structure. Multibeam TEM image (right) of a similar area, in the thinnest part of the specimen, showing big nanoparticles with modified contrast (A) and modified morphology (B).*

In the thinnest areas of the XTEM specimen, the contrast of the big Ge nanoparticles changes showing an inner ring (nanoparticle A in Fig. 2). Some nanoparticles appear with a modified shape (nanoparticle B in Fig. 2) due to the ion thinning process, in the very thin areas of the specimen. Fig. 2 also shows a network of amorphous small Ge nanoparticles with sizes between 3 and 5 nm, uniformly distributed in the film volume. Some particles have intermediate sizes, between 5 and 15 nm, but they are probably formed by aggregation of several small nanoparticles, as the images contrast suggests. The main part of Ge species present in the film segregates in these small amorphous nanoparticles and only few percents of Ge content form the big Ge nanoparticles.

Detailed observations at high magnification taken in areas of the XTEM specimen with thickness similar with the size of big Ge nanoparticles (about 50 nm) show (Fig. 3) a Ge depleted zone around the big nanoparticle. In this depleted zone, the SiO<sub>2</sub> matrix is clear and no small Ge nanoparticles are present.

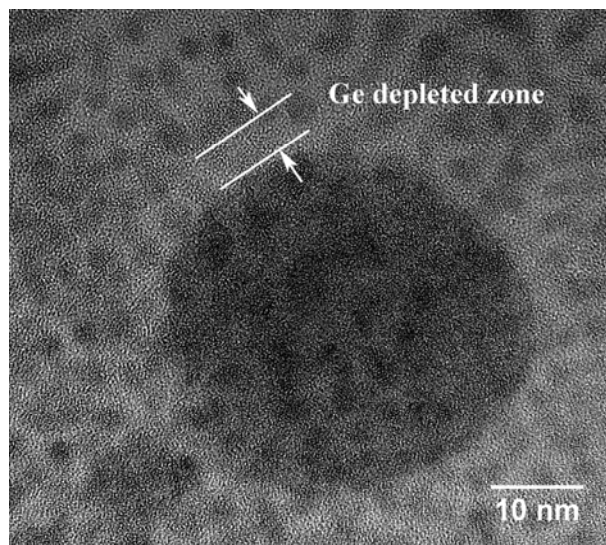


*Fig. 3. HRTEM image of a round big Ge nanoparticle (40 nm) and the network of the amorphous small Ge nanoparticles.*

In the very thin area of the XTEM specimens, the big Ge nanoparticles are not spherical (Figs. 2 and 4a). In such areas it is possible to record high resolution images of the big Ge nanoparticle structure showing 0.27 nm lattice fringes. They are not stable under electron irradiation and the lattice fringes contrast disappears in several seconds. However, the lattice fringe image can be recorded in view mode, at the expense of a lower quality (see Fig. 4b).

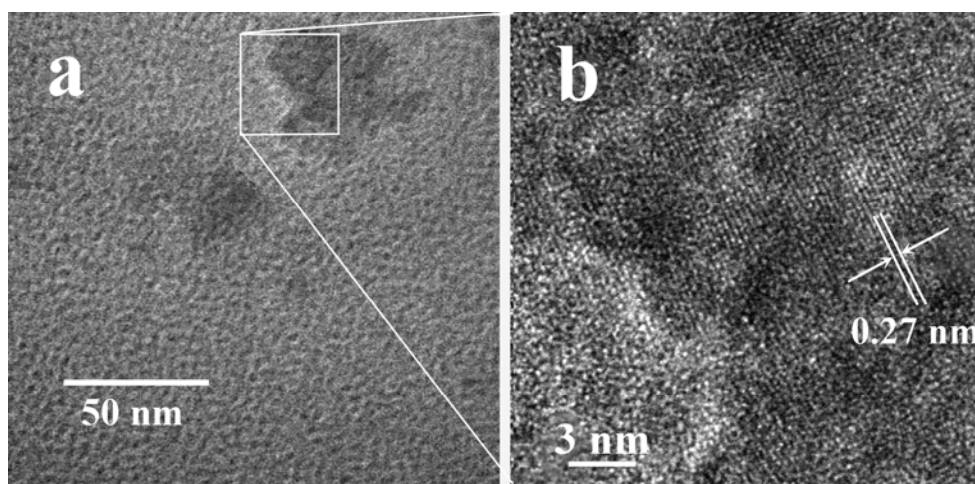


*Fig. 4. Multibeam XTEM image of a big Ge nanoparticle with irregular shape (a) taken in a very thin area of the specimen. The HRTEM detail (b) shows the presence of the 0.27 nm lattice fringes, corresponding to the strongest (201) reflexion of the tetragonal Ge.*

Figs. 5 a and b show the same area of the specimen in the beginning of the HRTEM observations (see Fig. 5a), and after about one minute when the image becomes stable (see Fig. 5b). In the beginning, the 0.27 nm lattice fringes are visible, then the lattice fringes disappear, and in about one minute the 0.2 nm lattice fringes corresponding to the diamond cubic structure of Ge-I appear.

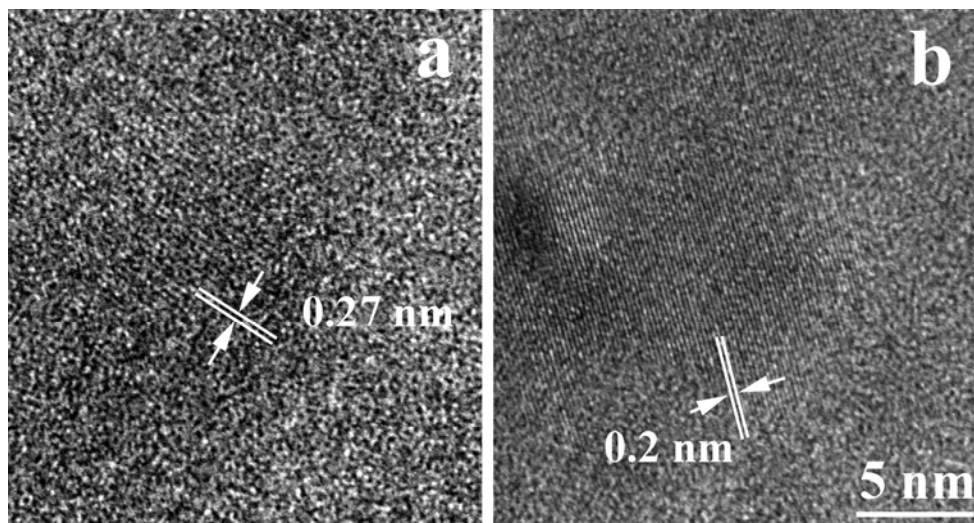


Fig. 5. HRTEM images of an initial area (a) showing 0.27 nm lattice fringes of Ge-III phase. This area becomes amorphous in several seconds and then re-crystallizes in the cubic structure (b) and the HRTEM image becomes stable.

As mentioned before, the small Ge nanoparticles, forming the dense uniform network in the film volume are amorphous. These amorphous nanoparticles appear as spherical dark contrast nanoregions (Fig. 6).

The EDX measurements with the electron probe (3 nm) centered in a dark nanoregion, i.e. centered on a small Ge nanoparticle, give a value of about 3.5 for the Ge/Si atomic ratio [40]. These results indicate the major presence of Ge atoms in the dark nanoregions, confirming that the small amorphous nanoparticles are really of Ge.

Some of the small Ge nanoparticles show lattice fringes like contrast, corresponding to the (111) lattice spacing of the cubic Ge (see Fig. 6b). However, even the recording of the HRTEM image happens fast, in the very beginning of the specimen observation the effect of Ge nanoparticle crystallization induced by the electron beam irradiation is also fast. So we cannot really see at high resolution the initial structure of these small Ge nanoparticles without any electron irradiation effect.

This effect of the electron irradiation upon the specimen can be easily seen by imaging in low magnification the specimen area where the high resolution imaging was performed before (see Fig. 6c). Fig. 6c also shows the ripening effect of the electron irradiation. This effect is known for the GeSiO system which is very sensitive to the electron beam-irradiation [41, 42]. In the irradiated area, the Ge nanocrystallites are crystallized in the diamond cubic structure as revealed by the high resolution images shown in Fig. 6b. At this stage, the HRTEM images become stable under the electron beam.

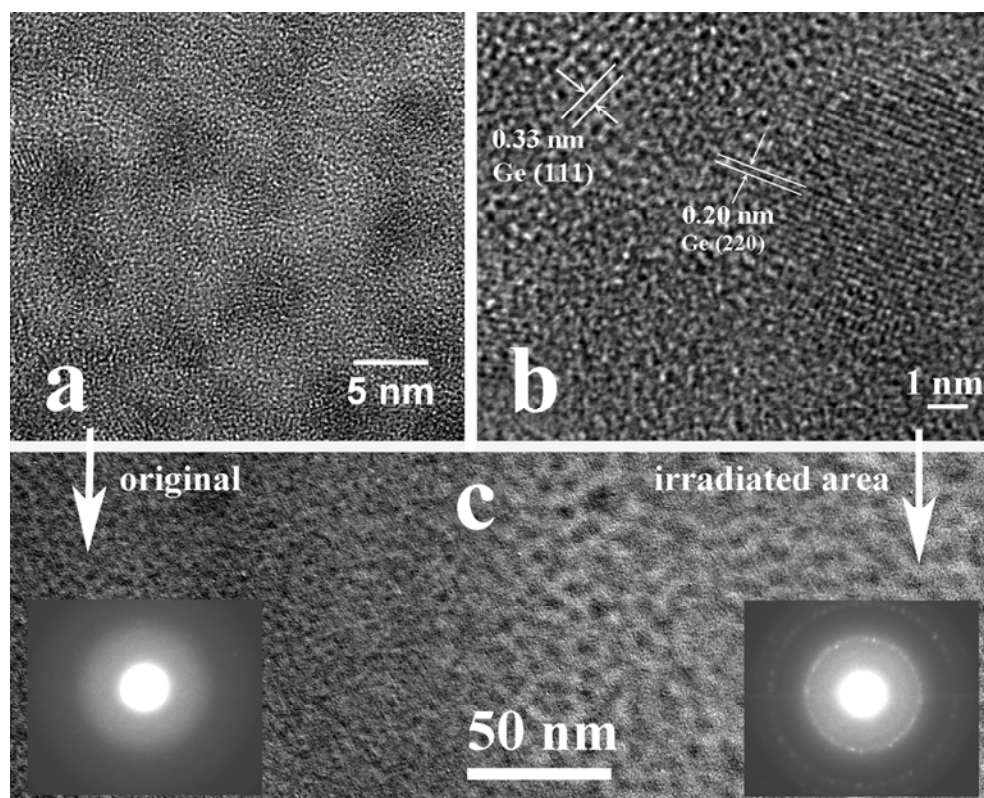


Fig. 6. (a). High magnification HRTEM image of the small Ge nanoparticles, corresponding to the dark contrast nanoregions network. The nanoparticles are amorphous, but some of them show the lattice fringes contrast corresponding to the cubic Ge. (b). HRTEM image showing the cubic Ge crystallization in the dark nanoregions under the electron irradiation. Lattice fringes correspond to (111) (0.326 nm) and (220) (0.2 nm) of cubic Ge structure. (c). Low magnification TEM image showing modification of the specimen structure, after several minutes of HRTEM observation. In the modified area the Ge nanoparticles are bigger and crystallized in the cubic phase.

In order to establish the evolution of the GeSiO film structure during subsequent annealing, the samples were heated at 800 °C in nitrogen atmosphere. This evolution is illustrated in Fig. 7 which shows the film structure after both the first and the second annealing, in the region of interface with the quartz substrate where the density of the Ge nanoparticles is higher than in the film volume.

This high density of Ge nanoparticles near the SiO<sub>2</sub>/Si interface is due to the mobility of the Ge in the film structure, which goes out from the film volume. So, the Ge diffusion stops near the substrate interface and forms a quasicontinuous layer separated from the substrate by a several nanometres thick SiO<sub>2</sub> layer, this effect being observed in many papers [25, 39, 42].

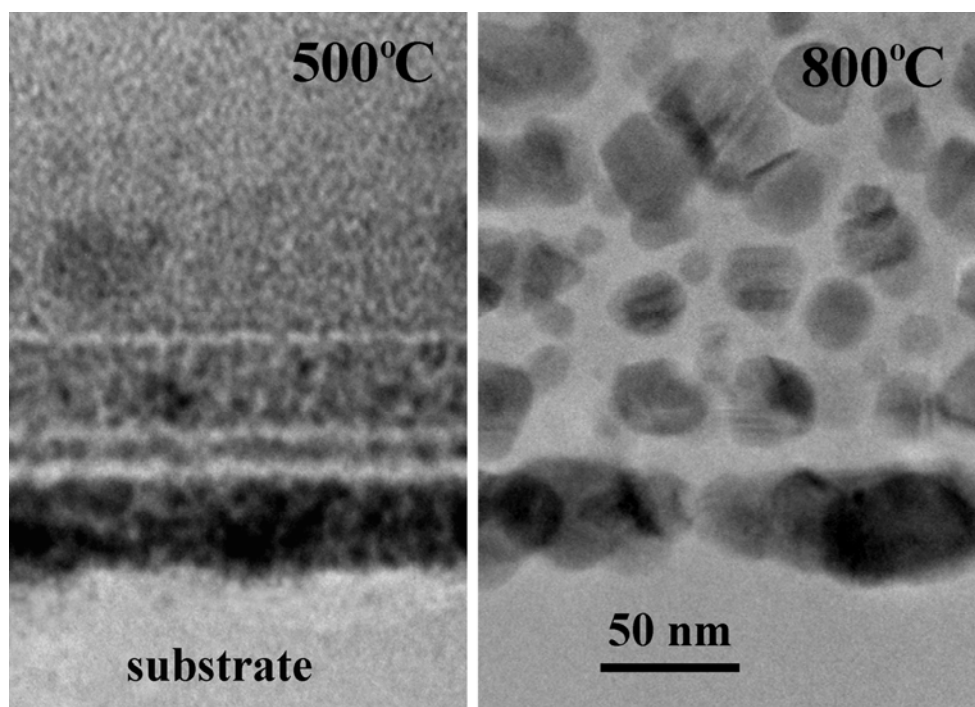


Fig. 7. (a). Low magnification TEM images comparing the film structure at the interface with the quartz substrate, after the first annealing at 500 °C in  $H_2$  and after the second annealing in  $N_2$  at 800 °C. At the interface region between the film and the substrate the density of the nanoparticles is higher than in the film volume forming a quasicontinuous layer.

After the annealing at 800 °C, the two types of morphology for the Ge nanoparticles disappear, so that all Ge crystallites have the same morphology. In this case, the Ge crystallites are faceted (Figs. 7 and 8), they have the diamond cubic structure (Ge-I) and sizes between 20 and 50 nm. Fig. 8 shows a high resolution image of a cubic Ge nanoparticle near [110] orientation. The Ge crystallites show inside defects as stacking faults and nanotwins and have mainly (111) facets.

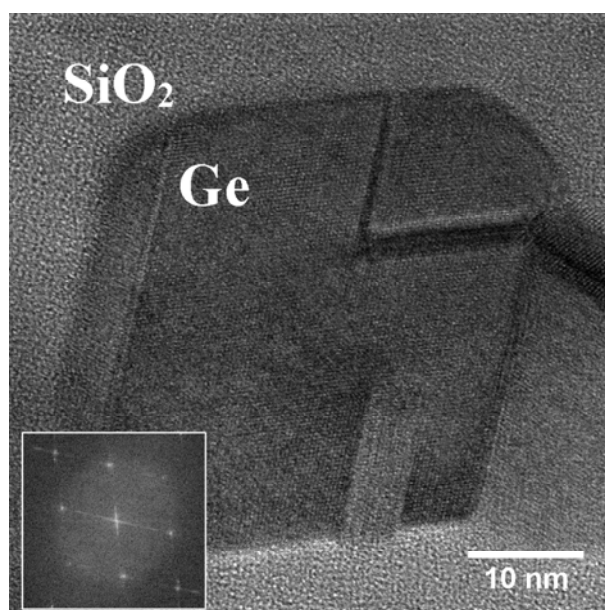


Fig. 8. HRTEM image of a cubic faceted Ge nanocrystallite after the sample annealing in  $N_2$  at 800 °C. The inset fast Fourier transform pattern indicates the [110] close orientation of the structure.

The presence of the two types of Ge nanoparticles after annealing in hydrogen suggests the presence of two types of segregation mechanisms by which the big Ge nanoparticles and the uniform network of amorphous small Ge nanoparticles are formed. In the first mechanism, the segregation can start from existing Ge nuclei, originating from the fluctuation of local Ge concentration and having enough time to collect many Ge species, leading to the formation of big round nanoparticles with a well defined interface between them and SiO<sub>2</sub> matrix. The second mechanism is a uniform nucleation of Ge clusters in all the film volume, leading to the formation of the small Ge nanoparticle network. After the uniform nucleation, the Ostwald ripening process can work inducing a separation between the big Ge nanoparticles and the network of small Ge nanoparticles by formation of the depleted zone around the big nanoparticles (Fig. 3). The annealing in H<sub>2</sub> at 2 atm and 500 °C is not sufficient to crystallize the network of small Ge nanoparticles. Probably in this case, the small Ge nanoparticles contain unreduced GeO<sub>x</sub> which prevents the crystallization process. In the literature, the crystallization of Ge nanoparticles is reported at higher temperatures, between 700 and 900 °C [39, 43].

The high density electron irradiation during HRTEM observations increases the local temperature but also increases the local diffusion of the species due to the irradiation enhanced diffusion effect. This can produce a relaxation of the local irradiated area and destabilizes the metastable Ge-III phase present in the specimen structure. This can explain the rapid amorphisation of the tetragonal Ge structure under the electron irradiation. However, this effect does not happen in the case of ST12 (Ge-III) Ge nanoparticles obtained by chemical route [33]. A better stability of the free small nanoparticles under electron irradiation is a known effect, previously observed on AgCl nanoparticles [44].

On the other hand, during the ion thinning process performed for the XTEM specimen preparation, the very thin area of the specimen partially relaxes. Thus the tetragonal Ge crystallites can become partially amorphous. This process is not complete and some lattice fringes can be observed after ion thinning. Consequently, the total crystallinity of the sample becomes too low to be revealed by the SAED patterns. Also, during the ion thinning, the spherical shape of the Ge-III nanoparticles becomes irregular in the areas where the specimen thickness is less than the Ge-III particle size.

In the case of TEM specimens prepared by the extraction of microfragments from the film [13], the observed transparent areas on the edges of the fragments are much thicker and the film structure relaxation is probably limited, keeping more Ge-III phase enough for the SAED collection data.

More than that, the high pressure phases induced by diamond indentation are demonstrated to be stable for the film kept on the substrate and are probably less stable or they are not present in the detached microfragments. Our experience on microfragments obtained from oxide films deposited on silicon substrate using diamond tip extraction shows the presence of a lot of defects in the silicon substrate, but not the presence of a high pressure phase of silicon. So, in our opinion, the Ge-III phase found in the film microfragments is induced by the annealing process and not by the TEM specimen preparation.

In any case, the presence of traces of the Ge-III phase in the XTEM specimens shows that this phase already exists in the annealed film. The XTEM preparation method can only partially destroy this phase during specimen preparation.

The major part of Ge (about 40%) is segregated in the small amorphous Ge nanoparticles network. This network is responsible for the conduction mechanism in the sample, as we already demonstrated [40]. It is difficult to consider that all these nanoparticles are only amorphous. The problem is that the GeSiO system is very sensitive to the electron beam irradiation and these nanoparticles crystallize very fast in the cubic diamond structure of Ge. Even if we used the electron beam with its smallest intensity which makes possible high resolution imaging, the crystallization effect becomes visible in seconds.

Finally, we can imagine the following scenario. The initial deposited GeSiO film with amorphous structure has some important fluctuations of local concentration of Ge species which probably result from the nonuniform structure of the target (SiO<sub>2</sub> target with Ge pieces attached). In the areas with maximum Ge concentration, the local stress field and the Ge supersaturation are also high. This leads to the formation of local Ge nuclei built on the existing Ge clusters which can

have a different structure in respect to Ge-I. At the beginning of the annealing process in H<sub>2</sub>, these nuclei grow, collect the Ge species from the surrounding area and become big Ge nanocrystals with Ge-III structure and spherical morphology. So, the formation of big Ge nanocrystals with Ge-III structure relaxes the stress field in the matrix and the homogeneous nucleation which takes place in the whole film volume by Ge species segregation leads to the formation of the network of small amorphous Ge nanoparticles.

In our opinion, the relatively large thickness of GeSiO films (2.5 μm) together with the annealing conditions we have chosen (H<sub>2</sub> at 2 atm and 500 °C) are favourable factors for the formation of the big Ge nanocrystals with Ge-III structure in our films.

#### 4. Conclusions

We conclude that the presence of the metastable tetragonal high pressure (Ge-III/ST12) phase of Ge in the H<sub>2</sub> annealed film structure is due to the generation of a local stress field. This stress field is produced by the Ge segregation processes during annealing in the GeSiO films in the places where the initial concentration of Ge species has maximum fluctuation value. These places act as initial nuclei for the Ge segregation and growth of the big Ge nanoparticles. As the stress field is quite low, the growth of Ge-III phase is possible only by a mechanism related to the structure of the initial Ge clusters in the deposited GeSiO film, which can be different from the structure of a Ge cluster formed by thermal nucleation. The high resolution observations of these structures induce the amorphisation of the metastable Ge-III phase and finally the crystallization of the amorphous Ge nanoparticles in the stable cubic Ge-I structure. The subsequent annealing at 800 °C in N<sub>2</sub> relaxes the structure and the high diffusivity of Ge atoms at this temperature leads to the nucleation and growth of the faceted Ge nanocrystals with the diamond cubic (Ge-I) structure.

This work shows that the TEM specimen preparation method and the TEM observations conditions are important for the correct estimation of the structure.

#### Acknowledgements

The contribution to this work was supported by the Romanian National Authority for Scientific Research through the CNCS–UEFISCDI Contract No. PN II-PT-PCCA-9/2012.

#### References

- [1] P. Castrucci, S. Del Gobbo, E. Speiser, M. Scarselli, M. De Crescenzi, G. Amiard, A. Ronda, I. Berbezier, *J. Non-Cryst. Solids*. **356**, 1940 (2010).
- [2] S. Cosentino, P. Liu, S. T. Le, S. Lee, D. Paine, A. Zaslavsky, D. Pacifici, S. Mirabella, M. Miritello, I. Crupi, A. Terrasi, *Appl. Phys. Lett.* **98**, 221107 (2011).
- [3] P. Liu, S. Cosentino, S. T. Le, S. Lee, D. Paine, A. Zaslavsky, D. Pacifici, S. Mirabella, M. Miritello, I. Crupi, A. Terrasi, *J. Appl. Phys.* **112**, 083103 (2012)
- [4] J. K. Shen, X. L. Wu, R. K. Yuan, N. Tang, J. P. Zou, Y. F. Mei, C. Tan, X. M. Bao, G.G. Siu, *Appl. Phys. Lett.* **77**, 3134 (2000).
- [5] B. Zhang, S. Shrestha, P. Aliberti, M. A. Green, G. Conibeer, *Thin Solid Films* **518**, 5483 (2010).
- [6] S. K. Ray, S. Maikap, W. Banerjee, S. Das, *J. Phys. D: Appl. Phys.* **46**, 153001 (2013).
- [7] S. H. Hong, M. C. Kim, P. S. Jeong, S. H. Choi, K. J. Kim, *Nanotechnology* **19**, 305203 (2008).
- [8] B. Li, J. L. Liu, *Thin Solid Films* **518**, S262 (2010).
- [9] S. Cosentino, S. Mirabella, M. Miritello, G. Nicotra, R. Lo Savio, F. Simone, C. Spinella, A. Terrasi, *Nanoscale Res. Lett.* **6**, 135 (2011).
- [10] Y. X. Jie, A. T. S. Wee, C. H. A. Huan, Z. X. Shen, W. K. Choi, *J. Appl. Phys.* **109**, 033107 (2011).
- [11] I. Stavarache, A. M. Lepadatu, V. Teodorescu, T. Stoica, I. Pasuk, G. Stan, V. Iancu, M. L. Ciurea, *Proc. IEEE CN CFP10CAS-PRT, Int. Semicon. Conf. CAS 2010*, **1**, 77 (2010).
- [12] I. Stavarache, A. M. Lepadatu, M. L. Ciurea, *Proc. IEEE CN CFP11CAS-PRT, Int. Semicon. Conf. CAS 2011, Vol. 1*, 31 (2011).

- [13] I. Stavarache, A. M. Lepadatu, N. G. Gheorghe, R. M. Costescu, G. E. Stan, D. Marcov, A. Slav, G. Iordache, T. F. Stoica, V. Iancu, V. S. Teodorescu, C. M. Teodorescu, M. L. Ciurea, *J. Nanopart. Res.* **13**, 221 (2011).
- [14] I. Stavarache, A. M. Lepadatu, T. Stoica, M. L. Ciurea, *Appl. Surf. Sci.* **285B**, 175 (2013).
- [15] B. Zhang, Y. Yao, R. Patterson, S. Shrestha, M. A. Green, G. Conibeer, *Nanotechnology* **22**, 125204 (2011).
- [16] L. L. Araujo, R. Giulian, D. J. Sprouster, C. S. Schnohr, D. J. Llewellyn, P. Kluth, D. J. Cookson, G. J. Foran, M. C. Ridgway, *Phys. Rev. B* **78**, 094112 (2008).
- [17] R. Ang, T. P. Chen, M. Yang, J. I. Wong, M. D. Yi, *J. Phys. D: Appl. Phys.* **43**, 015102 (2010).
- [18] Q. Chen, T. Lu, M. Xu, C. Meng, Y. Hu, K. Sun, I. Shlimak, *Appl. Phys. Lett.* **98**, 073103 (2011).
- [19] S. Mirabella, S. Cosentino, A. Gentile, G. Nicotra, N. Piluso, L. V. Mercaldo, F. Simone, C. Spinella, A. Terrasi, *Appl. Phys. Lett.* **101**, 011911 (2012).
- [20] F. Gao, M. A. Green, G. Conibeer, E. C. Cho, Y. D. Huang, I. Pere-Wurfl, C. Flynn, *Nanotechnology* **19**, 455611 (2008).
- [21] C. M. Zhen, Y. B. Liu, L. Ma, Z. G. Pang, C. F. Pan, D. L. Hou, *J. Appl. Phys.* **107**, 043901 (2010).
- [22] C. Uhrenfeldt, J. Chevallier, A. N. Larsen, B. B. Nielsen, *J. Appl. Phys.* **109**, 094314 (2011).
- [23] A. Hernández-Hernández, V. T. Rangel-Kuoppa, T. Plach, F. De Moure-Flores, J. G. Quiñones-Galván, J. Santoyo-Salazar, M. Zapata-Torres, L. A. Hernández-Hernández, M. Meléndez-Lira, *J. Appl. Phys.* **111**, 044327 (2012).
- [24] A. M. Lepadatu, T. Stoica, I. Stavarache, V. S. Teodorescu, D. Buca, M. L. Ciurea, *J. Nanopart. Res.* **15**, 1981 (2013).
- [25] T. F. Stoica, M. Gartner, V. S. Teodorescu, T. Stoica, *J. Optoelectron. Adv. Mater.* **9**, 3271 (2007).
- [26] A. Alessi, S. Agnello, Y. Ouerdane, F. M. Gelardi, *J. Phys. Condens. Matter.* **23**, 015903 (2011).
- [27] S. Knebel, A. Kyriakidou, H. Bracht, H. Rösner, G. Wilde, *Appl. Phys. A* **103**, 149 (2011).
- [28] A. M. Lepadatu, I. Stavarache, T. F. Stoica, M. L. Ciurea, *Dig. J. Nanomater. Bios.* **6**, 67 (2011).
- [29] A. Rodríguez, B. Morana, J. Sangrador, T. Rodríguez, A. Kling, M. I. Ortiz, C. Ballesteros, *Superlattice. Microst.* **45**, 343(2009).
- [30] F. Bundy, J. S. Kasper, *Science* **139**, 340 (1963).
- [31] J. S. Kasper, S. M. Richard, *Acta. Crystallogr.* **17**, 752 (1964).
- [32] F. Coppari, J. C. Chervin, A. Congeduti, M. Lazzeri, A. Polian, E. Principi, A. Di Cicco, *Phys. Rev. B* **80**, 115213 (2009)
- [33] S. J. Kim, O. K. Quy, L. S. Chang, E. A. Stach, C. A. Handwerker, A. Wei, *J. Mater. Chem.* **20**, 331 (2010).
- [34] V. S. Teodorescu, M. G. Blanchin, *Microsc. Microanal.* **15**, 15 (2009).
- [35] G. Patriarche, E. Le Bourhis, M. M. O. Khayyat, M. M. Chaudhri, *J. Appl. Phys.* **96**, 1464 (2004).
- [36] D. J. Oliver, J. E. Bradby, S. Ruffell, J. S. Williams, P. Munroe, *J. Appl. Phys.* **106**, 095309 (2009).
- [37] I. D. Sharp, D. O. Yi, Q. Xu, C. Y. Liao, J. W. Beeman, Z. Liliental-Weber, K. M. Yu, D. N. Zakharov, J. W. Ager, D. C. Chrzan, E. E. Haller, *Appl. Phys. Lett.* **86**, 063107 (2005).
- [38] A. Wellner, V. Paillard, C. Bonafos, H. Coffin, A. Claverie, B. Schmidt, K. H. Heinig, *J. Appl. Phys.* **94**, 5639 (2003).
- [39] H. G. Chew, F. Zheng, W. K. Choi, W. K. Chim, Y. L. Foo, E. A. Fitzgerald, *Nanotechnology* **18**, 065302 (2007).
- [40] I. Stavarache, A. M. Lepadatu, A. V. Maraloiu, V. S. Teodorescu, M. L. Ciurea, *J. Nanopart. Res.* **14**, 930 (2012).
- [41] M. Klimenkov, W. Matz, J. von Borany, *Nucl. Instrum. Meth. Phys. Res. B* **168**, 367(2000).
- [42] W. K. Choi, Y. L. Foo, V. Ho, R. Nath, *Chem. Phys. Lett.* **416**, 381 (2005).
- [43] Y. Maeda, *Phys. Rev. B* **51**, 1658 (1995).
- [44] C. Goessens, D. Schryvers, R. De Keyzer, J. Van Landuyt, *Electron Microscopy, EUREM 92*, Granada, Spain, Vol. **2**, 649 (1992).